DESIGN AND VERIFICATION OF AN OSCILLATING WEAR TESTER TO SIMULATE THE PISTON-CYLINDER TRIBOLOGY IN INTERNAL COMBUSTION ENGINES

BY

BHAA ALDEN HUSSEIN ALI AL- TMEEMI

Thesis submitted in fulfillment of requirements for the degree of

Master of Science (Research Mode)

JANUARY 2011

DESIGN AND VERIFICATION OF AN OSCILLATING WEAR TESTER TO SIMULATE THE PISTON-CYLINDER TRIBOLOGY IN INTERNAL COMBUSTION ENGINES

BHAA ALDEN HUSSEIN ALI AL- TMEEMI

UNIVERSITI SAINS MALAYSIA

2011

ACKNOWLEDGMENTS

In the name of Allah, the most Beneficent, the most Merciful

Thanks to Allah who has helped me to carry out this study

Thanks to the first teacher Prophet Muhammad, peace is upon him and on his pure, pious family.

First of all, I would like to express my sincere thanks to my beloved and venerable mother who has helped me in her prayers for my success, to her I am greatly indebted for life for her sacrifices and motivation, and I dedicate my certificate to her. I would like to thank my supervisor, Professor Dr. Horizon Walker Gitano-Briggs, for his support and motivation throughout this research work. I wish especially to thank my brother and my teacher Amir H. Ali, Ph.D. student for his help and support. In addition, I wish to thank my brothers and my sisters for their continuous support to overcome all the difficulties that I faced while completing this work. Special appreciation and thanks to my beloved wife and my beloved children who endured many difficulties and shouldered various responsibilities during my absence. Once again, I would like to thank all the staff of the School of Mechanical Engineering. And I want to thank my friends and colleagues in my company who had always helped me. Last, I request from Allah to protect all these people who have helped me during my study.

TABLE OF CONTENTS

page

Acknowledgements i

Table of Contents ii

List of Tables vi

List of Figures vii

List of Symbols xiii

List of Abbreviations xvii

Abstrak xix

Abstract xxi

CHAPTER 1: INTRODUCTION

1.1 Introduction 1

1.2 Background of research. 1

1.2.1 Tribology. 1

1.2.2 Friction. 2

1.2.3 Friction under lubricated conditions. 4

1.2.4 Wear 6

1.3 Problem statement. 6

1.4 The objectives of this research. 7

1.5 Scope of this study 7

CHAPTER 2: LITERATURE REVIEW

2.1 Introduction. 8

2.2 Overview of friction and wear measurement devices. 8

2.3 Methodologies, Analysis and measurements for friction and wear. 12

2.4 Summary. 43

CHAPTER 3: EXPERIMENTAL SET-UP AND METHODOLOGY

3.1 Introduction. 45

3.1.1 Surface topography. 45

3.2 The procedure and set-up of Oscillating Wear Tester fabrication. 48

3.2.1 Design and fabrication. 48

3.2.1(A) Load system. 49

3.2.1(B) Motion system. 51

3.2.1(C) Frictional force measurement system. 52

3.2.2 Analysis and calculations 54

3.2.2(A) Calculation of spring stiffness. 54

3.2.2(B) Calculation of springs stiffness (center spring). 55

3.2.2(C) Calculation of springs stiffness (bottom springs). 56

3.2.2(D) Strain gauge properties. 56

3.2.2(E) Machines and Instruments used to fabricate OWT. 57

3.2.2(F) Sample preparations before testing. 57

3.2.2(G) Calculation of spring strain plate's thickness to provide 2 kHz frequency. 60

3.2.2(H) Stiffness calculation of the spring thickness 2.3 mm. 63

3.2.2(I) Calibration of spring strain plate of thickness 2.3mm.63

3.2.2(J) Geometrical analysis of the oscillating wear tester motion. 65

3.2.2(K) Method of wear calculation. 67

3.2.3 Set up and working of (OWT). 69

3.2.3(A) Set up and connecting the (OWT). 69

3.2.3(B) Experimental of this study. 70

Chapter 4: RESULTS AND DISCUSSION

4.1 Introduction. 73

4.2 X-ray analysis of the blanks. 73

4.3 Stress and deformation analysis of assembly (spring strain plat, blank and base) 74

4.4 Calculation of resistance change (Δr) in the strain gauge. 77

4.5 Study of coefficient of friction (COF) with different Ra. 78

4.6 Study of COF behavior with different Loads. 81

4.7 Investigation of COF with the Time. 82

4.8 Study the relationship between the wear and Ra of four samples. 83

4.9 Study of the wear on slider with different quantities of oil. 85

4.10 Study of the wear on blanks with different quantities of oil. 87

4.11 Study of the temperature with different surface roughness. 90

4.12 Study of the temperature vs. RPM with different quantities of oil for blanks. 91

4.13 Study of the relationship between temperatures and time. 92

CHAPTER 5: CONCLUSIONS AND RECOMMENDATIONS.

5.1 Conclusion. 93

5.2 Recommendations 95

REFERENCE 96

PUBLICATIONS 101

LIST OF TABLES

		Page
Table 2.1	Details of the wear test conditions used in this study. (Basavarajappa et al. 2007)	12
Table 2.2	Variations of temperature and coefficient of friction at different Loads of the unreinforced alloy and composites after sliding distance of 1800 m (0.5h).(Daoud et al. 2004).	15
Table2.3	Physical and mechanical properties of Ti(N) ceramic. (Xingzhong et al. 1997).	21
Table2.4	Materials and Vickers hardness. (Jiangang et al. 2008).	26
Table 2.5	Flat surface treatments with their abbreviations. (Aldajah et al.(2005).	30
Table 2.6	Chemical composition of G- 3500.(Terheci et al. 1995).	37
Table 3.1	Properties of the strain gauge. (Manual Tokyo Sokki Kenkyuio co.,Ltd).	56
Table 3.2	Parts of oscillating Wear tester (OWT).	59

LIST OF FIGURES

		Page
Figure 1.1	Stribeck diagram for journal bearing.(John B. Heywood and Jack P.Holman ,1988).	5
Figure 2.1	Schematic drawing of reciprocating wear tester. (Dae-Hyun CHO, Young-Ze LEE, 2009).	9
Figure 2.2	Schematic diagram of ball-on-disk contact geometry for reciprocating sliding wear testing.(Liu et al.2007).	10
Figure 2.3	Piston skirt scuffing tester. (Wang et al. 2005).	11
Figure 2.4	Schematic diagram of the oscillating tester. (Yufeng et al. 1995).	11
Figure 2.5	The schematic view of the pin-on-disc apparatus. (Basavarajappa et al.2007) .	12
Figure 2.6	Microstructures of the Al–Si matrix alloy and composites. (Daoud et al.2004).	14
Figure 2.7	Variation of pin surface temperature with sliding distance for matrix alloy and composites (test load: 90 *N*). (Daoud et al.2004).	15
Figure 2.8	Relationship between coefficient of friction and load. (Daoud et al.2004).	16
Figure 2.9	Variation of friction and wear rate load for Al-Si eutectic alloy in 50% RH air. Results from Bai ,Biswas (11) are shown for comparison . (Yen and Ishihara 1996).	18
Figure 2.10	Variation in the coefficient of friction with speed. (Ravikiran and Surappa, 1997).	19

Figure 2.11	The variation of the friction induced temperature rise of the pin and the coefficient of friction with normal load for samples tested at constant velocity of 2.5m/s. (Edrisy et al.2001).	20
Figure 2.12	Scheme of contact model of the specimens. (Xingzhong et al.1997).	21
Figure 2.13	Variation of friction coefficient with load. (Xingzhong et al. 1997).	22
Figure 2.14	Variation of friction coefficient with speed. (Xingzhong et al.1997).	23
Figure 2.15	Experimental apparatus.(Dae Kyun Baek and Khonsari,2005).	24
Figure 2.16	Friction coefficient of fresh rubber as a function of load. (Dae Kyun Baek and Khonsari,2005).	25
Figure 2.17	Wear rate of AISI 304, Fe_3Si, Fe_3Si-5%Cu,and Fe_3Si-10%Cu sliding against Si_3N_4 as a function of load. (Jiangang et al. 2008).	27
Figure 2.18	Wear rats of Si_3N_4 ball sliding against AISI 304, Fe_3Si, Fe_3Si-5%Cu, and Fe_3Si-10%Cu as a function of load. (Jiangang et al.2008).	28
Figure 2.19	Friction coefficients of the four tribo-pairs as a function of load. (Jiangang et al. 2008).	29
Figure 2.20	Friction coefficient versus time for dry contact. (Aldajah et al.2005).	31

Figure 2.21 Ball wear volume. (Aldajah et al.2005). 32

Figure 2.22 a Variation of volumetric wear with the sliding distance for A390 tested in argon at loads 5, 10, and 30N (Elmadagli and Alpas , 2006). 34

Figure 2.22b Variation of COF with the sliding distance for A390 tested in argon at loads 5, 10, and 30N (Elmadagli and Alpas ,2006). 35

Figure 2.23 Schematic drawing of pin-on-disc settings. (Terheci et al. 1995). 36

Figure2.24 Typical friction diagram produced by the CSEM Tribometer at5N,500 rev/min. after 100 k cycle (arm length, 15 mm). (Terheci et al.1995). 38

Figure 2.25 Friction coefficient f vs. load (500rev/min; 100k cycles; 15 mm arm length). (Terheci et al.1995). 38

Figure 2.26 piston-ring friction force measuring system with slider mechanism. (Sung et al. 2000). 40

Figure 2.27 Estimated frictional modes for test ring (SAE 5W/30). (Sung et al. 2000). 41

Figure 2.28 Ring and cast iron weight loss after wear testing in various lubricants. (John et al. 2005). 42

Figure 3.1 Selected types of surface deviations relative to an ideal solid surface. (Peter, J., Blau and Scott D. Henry , 1992). 46

Figure3.2	Coordinates used for surface-roughness measurement using Eq.[3.1] and [3.2] (Serope and Prentice Hall.2006).	47
Figure 3.3	Measuring surface roughness with a stylus. (Serope and Prentice Hall. 2006).	47
Figure 3.4	Diagram for oscillating wear tester (OWT).	48
Figure 3.5	Oscillating Wear Tester.	49
Figure 3.6	Parts of Load system.	50
Figure 3.7	Parts of Motion system.	51
Figure 3.8	SolidWorks drawing for important parts of (OWT) .	52
Figure 3.9	Parts of frictional force measurement system.	53
Figure 3.10	Calculation of spring stiffness.	54
Figure 3.11	A signal by using spring strain plate with thickness 0.7mm, RPM750.	60
Figure3.12	A signal by using spring strain plate with thickness 2.3mm, RPM750.	62
Figure 3.13	Photo for the calibration procedure.	64
Figure3.14	Spring strain gauge calibration.	64

Figure 3.15	a-Diagram of sliding motion for the specimen on the blank, b-and c-geometrical analysis.	66
Figure 3.16	Mode of linear velocity at RPM750.	66
Figure 3.17	Sketch of the wear on the blank.	67
Figure 3.18	Photo of Alicona testing includes the depth of wear.	68
Figure 3.19	Diagram for Oscillating Wear Tester setup.	69
Figure 3.20	Flow chart explaining the working mechanism of the oscillating wear tester.	72
Figure 4.1	X-ray shows components of metal (AL 380.0-F Die casting alloy).	74
Figure 4.2a	Cosmos Work stress analysis.	75
Figure 4.2b	Cosmos Work deformation analysis.	76
Figure 4.3	Relationship between Friction force and Time for RPM750, Load 112N, lubricant 1.01g and *Ra* 117.38 nm.	79
Figure 4.4	Relationship between Friction force and time for RPM 750, Load 112N, lubricant 1.01g and *Ra* 190.48 nm.	79
Figure 4.5	Relationship between Friction force and time for RPM 750, Load 112N, lubricant 1.01g and *Ra* 303.63 nm.	80
Figure 4.6	Relationship between Friction force and time for RPM 750, Load 112N, lubricant 1.01g and *Ra* 587.29 nm	80
Figure 4.7	Relationship between coefficient of friction and Ra (nm) for, RPM 750, Load 112N, lubricant 1.01g and Time 2h.	81

Figure 4.8 Relationship between COF vs. Load.RPM 750, *Ra* 155.7nm and oil 0.5g. 82

Figure 4.9 Relationship between COF vs. Time. RPM 750, *Ra* 130nm, Load 120N and oil1g. 82

Figure 4.10 Relationship between wear (mg) and Ra (nm) for, RPM 750, Load 112N, Lubricant 1.01g and Time 2h. 83

Figure 4.11 Photos by Alicona tester of samples with different Ra before and after the test. 84

Figure 4.12 Relationship between the wear and different quantities of oil for the slider.RPM 750, load 112N, time 2h and average *Ra* 130nm. 85

Figure 4.13 Slider Photos by Alicona tester before and after the wear test. 86

Figure 4.14 Relationship between wear vs.oil of blanks for, RPM 750, Load 112N, time 2h and Ra 172 nm. 88

Figure 4.15 Alicona photos of the wear with different quantities of oil for samples. 89

Figure 4.16 Relationship between Temperature °C vs. Ra nm.RPM 750, Load 112N, time 2h and lubricant 1.01g. 91

Figure 4.17 Relationship between temperatures vs. RPM with different quantities of oil for blanks. Load 112N, Ra 165nm and time 2h. 92

Figure 4.18 Relationship between temperature vs. time.RPM 750, Load 108N, Ra 104nm and oil 0.5g. 92

LIST OF SYMBOLS

(μ_G) Coefficient of friction in general.

(F) Friction force.

(μ_s) Static coefficient of friction.

(μ_k) Kinetic coefficient of friction.

(N) Normal load.

(f) Coefficient of friction.

(η) Dynamic viscosity.

(σ) Load force per unit area.

($\mathcal{N}$) Rotational speed.

(f_s) Dry friction.

(f_L) Hydrodynamic friction.

(α) Contact constant surface.

(Ra) Surfaces roughness.

(a.b.c) Absolute values.

(n) Number of reading.

(Rq) Root mean square.

(RPM) Revolution per minute.

(ρ) Density.

(D) Sliding distance.

(C) Constant= $EW/4L^3$.

(E) Young modulus for steel= $200x\ 10^9\ N.m^2$.

(K_1) Stiffness of center spring.

(K_2) Stiffness of bottom springs.

(ΔX) Difference of the length of spring before and after load.

(f_n) Natural frequency.

(ω_n) Angular frequency.

(π) pi=3.141.

(K) Gauge factor= 2.13.

(σ) Stress from simulation analysis= $1.1x10^7\ n/m^2$

(ϵ) Strain of spring strain gauge.

(r) Gauge resistance= 120 Ω.

(X) Position of specimen.

(ΔW) Weight loss.

(B) Width of wear scar.

(A) Area of cross section of worn surface.

(L_o) Oscillating stroke.

(S) Total sliding distance.

(d) Wear scar diameter.

(V) Liner Velocity.

(V_L) Volume loss.

(M_L) Mass loss.

(L_w) Length of wear.

(W_w) Width of wear.

(D_W) Depth of wear.

(K_{so}) Stiffness of old spring strain plate .

(T_{so}) Thickness of old spring strain plate.

(K_{sn}) Stiffness of the new spring strain plate.

(T_{sn}) Thickness of new spring strain plate.

(L) Length of linkage.

(R) Distance from the center of the pulley to point of linkage.

(f_1) Force from the center spring.

($2\ f_2$) Force from the bottom springs.

(X_o) Length of the spring before applying the load.

(X_1) Length of the spring after applying the load.

(S_s) The area of cross section.

(L_s) Length of the stroke.

(v_b) Ball wears volume.

($\mathcal{R}$) Ball radius.

(a) Acceleration.

(Δr) Change of resistance

(M_w) Mass of wear

LIST OF ABBREVIATIONS

(ICE)	Internal combustion Engine.
(H.V.)	Hardness Vickers
(HGA)	Head- Gimbal Assembly.
(SEM)	Scanning Electron Microscopy.
(Fig.)	Figure.
(LVDT)	Linear variable different transformer.
(LF)	Low frictional force.
(HF)	High frictional force.
(PTWA)	A plasma transfer wire arc.
(V_W)	Wear Volume.
(RH)	Humidity range.
(GFPL)	Glazed first then laser shock peened last.
(PFGL)	Laser shock Peening first then laser glazed last.
(COF)	Coefficient of friction.
(DLC)	Diamond-like carbon.
(DJ)	Diamond jet.

(OWT)	Oscillating Wear Tester.
(DAQ)	Data acquisition.
(Dia.)	Diameter.
(Go)	Laser glazed only.
(po)	Laser shock peend only.
(SRV)	Optimal reciprocating friction and wear tester.
(ASTM)	American society for Testing and Materials.
(SAE)	Society of Automotive Engineers.
(PPM)	Parts per million.
(XRD)	X-ray diffraction.
(EDXS)	Energy- dispersive x-ray spectroscopy.
(CLA)	Center line Average.
(AISI)	American Iron and Steel Institute.
(CSEM)	Commercially pin on disc machine.
(VFD)	Variable-frequency drive.

REKABENTUK DAN MENENTU-SAHKAN BAGI SEBUAH PENGUJI KEHAUSAN BERPUTAR UNTUK SIMULASI TRIBOLOGI PISTON-SILINDER DI DALAM ENJIN PEMBAKARAN DALAM

ABSTRAK

Satu penguji ayunan kehausan atau oscillating wear tester (OWT) dibina untuk simulasi kesan tribologi bagi piston silinder enjin pembakaran dalaman. Penguji OWT ini terdiri daripada beberapa sub-sistem iaitu sistem bebanan, sistem ayunan atau gerakan dan sistem pengukuran tekanan geseran. Ia beroperasi pada kelajuan di antara 10-1500 rpm. AL 380-0-F (die casting alloy) telah digunakan sebagai piston silinder dan bahan daripada keluli tahan karat (ring in piston ring assembly). Simulasi untuk 'spring strain plate, blank dan base assembly' telah dijalankan untuk mengetahui tekanan dan perubahan bentuk yang berlaku dengan menggunakan perisian 'SolidWorks dan CosmosWork'. Analisis geometri untuk pergerakkan specimen (piston silinder) telah dijalankan dengan menggunakan perisian MATLAB untuk mengetahui kadar lurus kelajuan pada 750 rpm. 'Strain gauge' telah digunakan untuk memindahkan isyarat tekanan geseran melalui amplifier kepada 'data acquisition' (DAQ) dan kemudian ke komputer dengan perisian komputer LabView. OWT telah digunakan untuk mengesahkan proses geseran dan kehausan. Banyak penyelidikan telah dibuat untuk mengetahui hubungan di antara pekali geseran (coefficient of friction - COF) dengan bebanan (load), kekasaran permukaan (surface roughness- Ra) dan masa (time). Hubungan di antara kehausan (wear) dengan Ra dan jumlah minyak yang berbeza juga dikaji. Selain itu, hubungan di antara suhu dengan Ra, masa dan jumlah pelincir yang berbeza juga

dijalankan. Keputusan menunjukkan COF berkurangan apabila beban meningkat, manakala ia meningkat apabila Ra meningkat dan berubah-ubah dengan masa. Sementara itu, kadar kehausan meningkat bila ra meningkat dan ia menurun bila kuantiti minyak meningkat. Selain itu, suhu meningkat apabila Ra, meningkat dan menurun apabila minyak meningkat. Suhu meningkat dengan masa selepas lebih kurang 35 minit ia mencapat kestabilannya.Semua keputusan ini diterima.

DESIGN AND VERIFICATION OF AN OSCILLATING WEAR TESTER TO SIMULATE THE PISTON-CYLINDER TRIBOLOGY IN INTERNAL COMBUSTION ENGINES

ABSTRACT

An Oscillating Wear Tester (OWT) was built to simulate the piston-cylinder tribology in internal combustion engines. This tester consists of load system, motion system and frictional force measurement system. It operates at a speed of 10-1500 rpm. AL 380-0-F die casting alloy used as blank (cylinder) and stainless steel specimen slider was fabricated as a ring in piston ring assembly. Simulation for the spring strain plate, blank and base assembly was conducted to find the stress and deformation by using SolidWorks, CosmosWork software. Geometrical analysis for the motion of the specimen on the blank of OWT was conducted by using MATLAB software to find the mode of linear velocity at 750 rpm. Strain gauge was used to transfer the signal of the frictional force throughout the Amplifier to data acquisition (DAQ) and then to the computer with LabView software. OWT was used to verify friction and the wear processes. Many studies were conducted to find the relationship between the coefficient of friction (COF) with load, surface roughness (Ra) and time. The relationship between the wear with (Ra) and different quantities of oil was studied. The relationship between temperature with Ra, time and different quantities of lubricant was studied. From the results, it can be found that the COF decreases when the load increases. Besides, COF rises when Ra increases and fluctuates with time. The wear increases with Ra increases and decreases when the quantity of oil increases. Also, the temperature increases with Ra increases and decreases with oil

increase. With the time, the temperature increases and after approximately 35 minutes, reached stability. All these results were acceptable .

CHAPTER 1

INTRODUCTION

1.1. Introduction

Despite the interest in protecting the environment from air pollution and the increase in fuel costs, the Internal Combustion Engines are still facing the problems of fuel consumption and smoke emission. Friction and wear play a very important role in the loss of energy, fuel consumption and smoke emission in internal combustion engines. Many researches and studies have been done with the aim to reduce friction and wear in engines.

1.2. Background of research.

1.2.1. Tribology.

Tribology studies have a long history, extending for a number of centuries before the word itself was coined in 1965. The first study about friction was done by Leonardo da Vinci in the late sixteenth century, and the first quantitative understanding of fluid film lubrication was listed by Beauchamp Tower at the end of the nineteenth century. The wide use of electron microscopy and other good methods of microanalysis improved the understanding of wear mechanism rapidly. Hutchings and Gwidon. (2005).It is essential to understand that in an engine the wear is a not a material property, but a tribological system property is. Marcia et al. (1998).

1.2.2. Friction.

Friction occurs when two surfaces come into contact with each other at several points. The force which resists or prevents the slipping or movement of surfaces with another is called ‘friction force’. This force is tangential to the surface of contact and it is opposite to motion directions of the surface relative to these points. In general, there are two types of friction that occurred between surfaces. They are dry friction and fluid friction. Dry friction occurs when there is no fluid (gas or liquid) of lubrication to separate two contacting surfaces. Fluid friction occurs when the contacting surfaces are separated by a film of fluid. According to Hibbeler and Prentice Hall. (2007). Friction plays an important and key role in many of the acts, such as starting the motion, the rotation and the stopping as well as in most manufacturing processes. Without friction, most threaded joints would not hold and friction welding would obviously not exist. On the other hand, friction causes loss of energy through heat. Cooling systems have been used to remove this heat to avoid damage to the machines. Some of this energy is dissipated in different deformation processes, such as the wear of the sliding surfaces. Friction is usually represented by the friction coefficient. In general, the friction coefficient (μ_G) is the ratio between the friction force (F) and the normal load (N)

$$\boldsymbol{\mu_G = F/N} \qquad \textbf{[1.1]}$$

The basic experimental laws that govern friction of solid bodies are quite simple and it must be emphasized that these laws are very general in nature and they are applicable in many situations. There are also many conditions in which they break down Peter,J., Blau and Scott D. Henry, (1992) . These laws were classified in general terms:

1-Static friction is greater than dynamic friction.

2-Friction is independent of sliding velocity.

3-Friction force is independent of contact area.

4-Friction force is proportional to applied load.

These laws are named after Coulomb, who formulated them in 1875, but much of his work was built on the earlier work of Leonardo da vinci and Amontons. Because of many mechanisms that contributed in generating the friction force, it's clear that the friction does not depend on the materials property alone, but it also depends on some extent of the measuring conditions, on the surface roughness, presence or absence of oxides or adsorbed films. In spite of these difficulties, the values of (μ_G) obtained through different methods and in laboratories tend to fall into ranges that are representative of the material pair in question under reasonably similar conditions Peter et al.(1992). A major part of the total energy loss in a reciprocating engine is due to piston ring and cylinder bore friction. According to Ozgen Akalin and Golam M.Newaz. (2001). The losses of friction in engine by the piston ring is about half of the total frictional losses roughly, within the power cylinder of an engine Jeffrey et al. (2006). The lubrication process of the piston ring-pack is affected by the engine friction and oil consumption Liang Liu and Tian Tian.(2005). One of the many solutions in obtaining good results such as low fuel consumption, low friction, high resistance of wear and to reduce the noise in engine that is to develop a structure of the piston with a new skirt structure. The good features for this piston were a skirt shape having optimal low rigidity and an optimum piston pin offset Naoki et al. (2002). The lubricant properties

are very important in lubrication system in engines. The variation of lubricant viscosity with shear rate, temperature and pressure determines how the lubricant performs in an engine Taylor. (2002). In most cases, a greater force is needed to set a resting body in motion than to sustain the motion. In other words, the static coefficient of friction (μ_s) is usually somewhat greater than the dynamic or kinetic coefficient of friction ($\mu_{k.}$). Peter et al.(1992).

1.2.3. Friction under lubricated conditions.

Many sliding surfaces are lubricated to protect against wear and to lower the friction. In a fully hydrodynamic situation, the lubricant film is sufficiently thick to keep the surfaces completely apart. Friction occurs due to viscous dissipation within the lubricant and has little or nothing to do with the nature of the contacting materials. As the two surfaces are brought closer together, the asperities begin to come in contact and the zone of so-called “boundary lubrication” emerges. Peter et al.(1992). The different regimes of lubricated friction can be illustrated by means of the Stribeck diagram shown in Figure 1.1, where the coefficient of friction (f) for a journal is plotted against a dimension less duty parameter $\eta\mathcal{N}/\sigma$ where (η) is the dynamic viscosity of the lubricant,($\mathcal{N}$) is the rotational speed of the shaft and (σ) is the loading force per unit area. John B. Heywood and Jack P.Holman (1988).

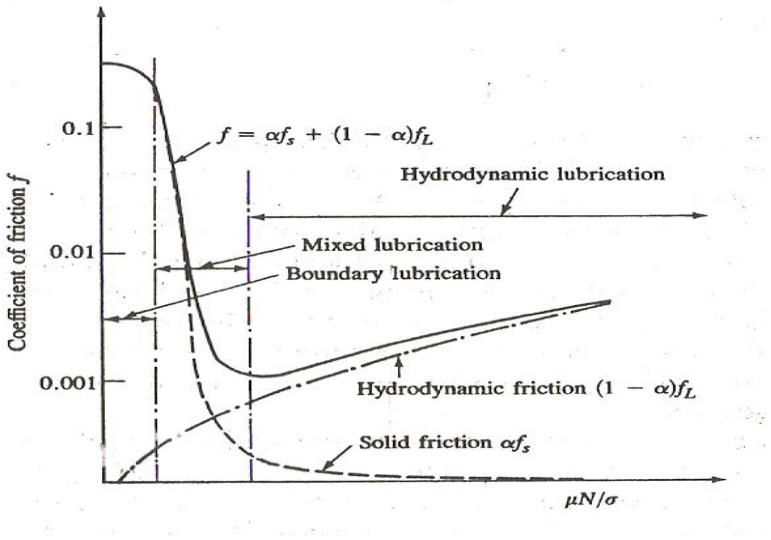

Fig.1.1: Stribeck diagram for journal bearing (John B. Heywood and Jack P.Holman 1988).

The coefficient of friction can be expressed in the following equation:

$$f = \boldsymbol{\alpha} f_s + (\mathbf{1} - \boldsymbol{\alpha}) f_L \qquad \textbf{[1.2]}$$

Where f_s is the metal-to-metal coefficient of dry friction, f_L is the hydrodynamic coefficient of friction, and α is the metal-to-metal contact constant, varying between 0 and 1 . As $\alpha \rightarrow 1$, $f \rightarrow f_s$ and the friction is called boundary, i.e., close to solid friction. The lubricating film is reduced to one or a few molecular layers and it cannot prevent metal-to-metal contact between the surface asperities. As $\alpha \rightarrow 0$, $f \rightarrow f_L$ and the friction is called hydrodynamic or viscous or thick film. The lubricant film is sufficiently thick in order to separate completely the surfaces in relative motion. In between these regimes, there is a mixed or partial lubrication regime where the transition from boundary to hydrodynamic lubrication occurs.

1.2.4. Wear

The definition of wear, which has been known for at least 50 years, includes the loss of material from a surface, transfer of material from one surface to another or movement of material within a single surface. A narrower definition of wear has been proposed as the progressive loss of substance from the operating surface of a body occurring as a result of relative motion at the surface Hutchings and Gwidon. (2005). The wide range of engineering applications of concern to the tribologist is served better by a broader definition. A simple and useful statement is that wear is harmful to a solid surface, usually involving progressive loss of material, because of the relative motion between that surface and contacting substances Hutchings and Gwidon. (2005). Some results show that, the shape of the piston groove significantly influences the amount of wear Sjodin and Olofsson. (2004).

1.3. Problem statement.

The major problems of Internal Combustion Engine (ICE) which affected the engine performance and fuel efficiency are friction and wear. Piston assembly and cylinder play main roles in this problem Leustek et al.(2005). To study these parameters, reciprocating friction and wear tester is usually used. The Oscillating Wear Tester (OWT) has been fabricated for this purpose. The (OWT) has some advantages including easy assembling and dismantling, relatively low cost compared with the commercial devices available. The latter which uses load cells costs approximately RM 10000 while OWT uses the spring strain plate which produces acceptable results. Al-Si cast alloys are widely used in automotive application because these alloys come with lighter weight, better heat conductivity than cast iron and high resistance of the wear.

So AL (380-0-F die casting alloy) has been used in this study by using the (OWT) which has been fabricated.

1.4. The objectives of this research.

A- To Design and fabricate Oscillating Wear Tester apparatus (OWT) to perform similar work for piston ring assembly and wall cylinder in reciprocating engines in Internal Combustion Engine (ICE).

B- To study the relationship between the coefficient of friction (COF), wear and temperature of AL (380.0-F die casting Alloy) as blank and stainless steel as slider with different variables. As well as a simulation for frictional force measurement system.

1.5. Scope of this study.

The Scope of this study was focused on the design and fabrication the Oscillating Wear Tester (OWT) and investigation of the coefficient of friction (COF) and wear of AL 380.0.F.Die casting with different variables.

CHAPTER 2

LITERATURE REVIEW

2.1. Introduction

Both friction and wear contribute to increase of fuel consumption and emission of gases that affect the environment. The frictional loss was estimated at about 25% of the overall fuel consumption in engines. Most of the frictional loss occurs on the sliding surface between the piston ring and cylinder block in the engine. There are many factors that are related to the friction and wear behavior of lubricated sliding surfaces, such as mechanical properties, sliding environments, chemical properties and surface properties. There are a lot of studies and researches devoted to the purpose of reducing the impact of friction and wear in the engines so far and it is still continuing Dae-Hyun CHO and Young-Ze LEE. (2009). Crankshaft, piston rings, cylinder, bearings, and the valve train are the important parts and the key in the work which needed the lubrication in a reciprocating engine. Light in weight and good design contribute to the process of control over the friction and wear and reduce them in the engines Zenon Krzyzak and Pawel Pawlus.(2006).

2.2 Overview of friction and wear measurement devices.

There are many ways and devices used to measure the friction and wear in internal combustion engine (ICE). The reciprocating wear tester is one of these important devices. It was used for the lubricated sliding tests. Figure 2.1. below shows the schematic drawing of the reciprocating wear tester. The dimensions of the specimens

of cylinder block used for the test were 4 mm × 4 mm× 60 mm, and that of the piston ring used for the test were 1.5 mm × 2.5 mm × 3.5mm.

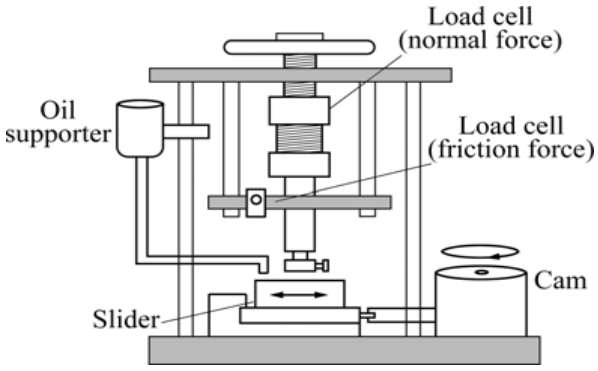

Fig.2.1: Schematic drawing of reciprocating wear tester. (Dae-Hyun CHO and Young-Ze LEE, 2009).

The ring was made of ductile cast iron, the block specimen, made of grey cast iron with a hardness of about HV 270, was held on the reciprocating table in a bath of oil Dae-Hyun CHO and Young-Ze LEE.(2009). There is another reciprocating sliding wear test. The displacement of the sample stage is a linear used to represent the samples frictional behaviors, where a ball-on-disk contact geometry was adopted as in Figure.2.2 below. The tester consisted of an XYZ - positioning system. The sample was mounted on an air-bearing carrier moving horizontally, and the vertical stage held a normal force actuator with a corundum ball of 10 mm diameter mounted at its lower end. A normal force is applied by compressing a double spring system against the ball. The counter body was horizontally connected to the stage by a quartz force transducer.

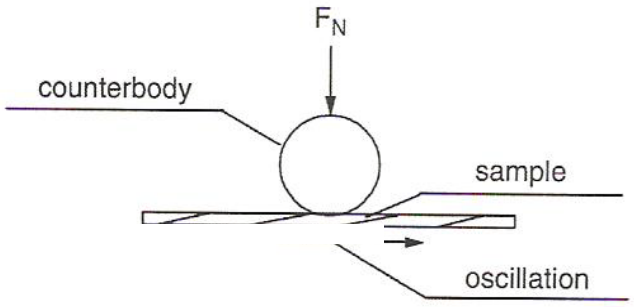

Fig. 2.2: Schematic diagram of ball-on-disk contact geometry for reciprocating sliding wear testing. (Liu et al. 2007).

Responding friction force, the linear contact displacement and the normal contact force were all measured as a function of time Liu et al.(2007). After developing the based on previous research, a piston scuffing bench tester was used to simulate the contact and lubrications between the piston and the cylinder bore. This tester consists of three important parts: driving system, loading system and lubrication system, as shown in Figure 2.3. It uses a speed-controllable motor to drive a single cylinder engine made by Briggs-Stratton to provide a vertical reciprocating motion of the cylinder bore sample. Through a pneumatic actuator, a horizontal adjustable load (normal load) is applied to push a piston sample against the bore sample through a loading block. A piston is installed on the piston holder through a horizontally placed pin and can rotate around or slide along the pin so that the piston has the self-centering capability with the bore sample and the piston skirt sustains the load against the bore sample only Wang et al .(2005).

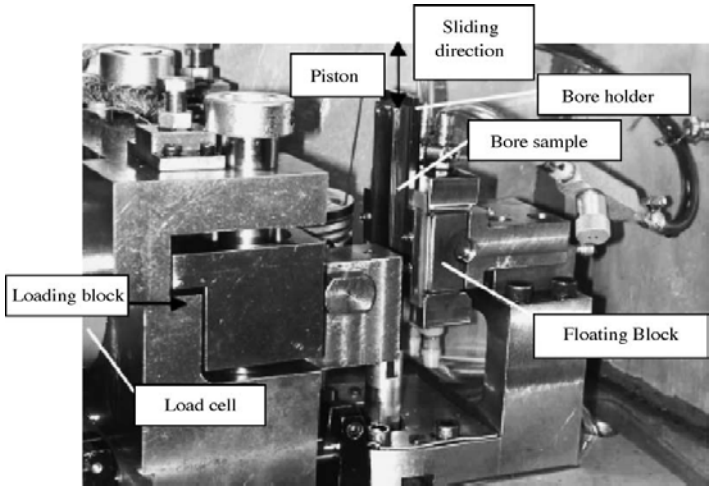

Fig. 2. 3: Piston skirt scuffing tester (Wang et al. 2005).

The oscillating tester is shown in Figure.2.4.it consists of a disk-mounting-stand, a dynamic force transducer, a dynamic exciter and an accelerometer. The disk to be tested was held by the disk-mounting-stand, and the dynamic exciter moves the head-gimbal assembly (HGA) sinusoidally. The dynamic force transducer and the accelerometer measure the instantaneous dynamic force (F_d) and an acceleration a of the (HGA) simultaneous Yufeng et al. (1995).

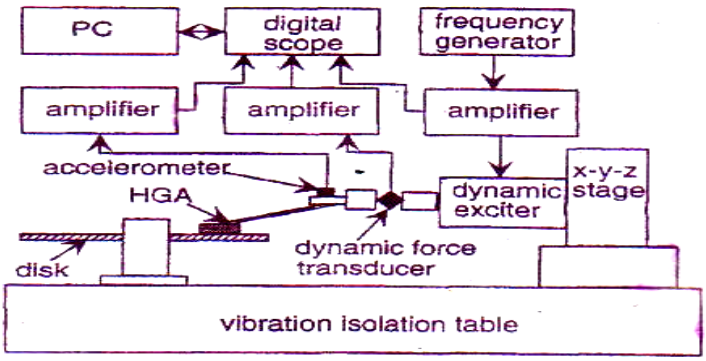

Fig.2.4: Schematic diagram of the oscillating tester. (Yufeng et al. 1995).

Figure 2.5 shows the schematic view of the pin on-disc apparatus which is used to conduct the dry sliding wear tests at room temperature as per the ASTM G9995 standards. The details of the wear test conditions are given in Table 2.1. Basavarajappa et al. (2007).

Table2.1:Details of the wear test conditions used in this study (Basavarajappa et al.2007)

Pin material	Al 2219, Al 2219/15SiCp, Al 2219/15SiCp-3Gr
Disc material	EN36 steel with a hardness of 65 HRc
Pin dimensions	Cylinder with diameter 10mm and height 30mm
Sliding speeds (m/s)	1.53, 3.0, 4.6, 6.1
Normal load (N)	40
Sliding distance (m)	5000

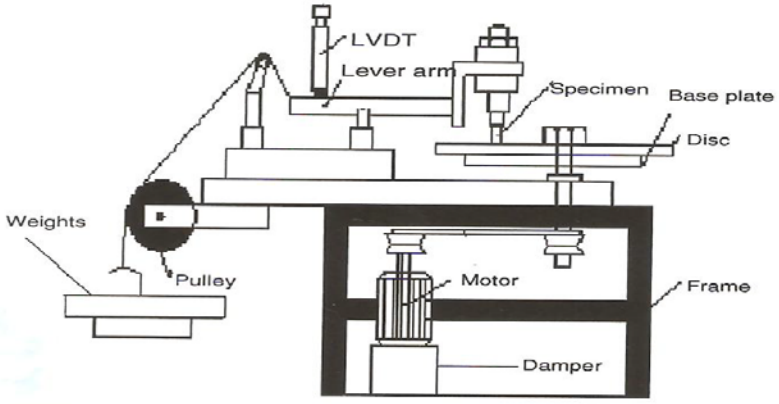

Fig.2.5: The schematic view of the pin-on-disc apparatus. (Basavarajappa et al.2007).

2.3 Methodologies, Analysis and measurements for friction and wear.

Al-Si alloy was used as the matrix material. The chemical composition of the matrix alloy in weight was Si 11.41%, Mg 1.54%, Ni 1.1%, Cu 0.982%, and the balance Al. Zro_2 or WC particles with an average size of 50 and 30 μm, respectively, were used as reinforcements. The stir-casting method was used to prepare the composites. Sliding

wear tests were carried out on a three pin-on-disk apparatus using a Falex-6 wear testing machine. The composites and the matrix alloy in the form of pins of 6 mm diameter and 15mm length were allowed to slide against a rotating disc of 60 mm diameter and 3 mm thickness. The Vickers hardness values of the investigated materials were 90, 105 and 103.5 HV for Al-Si, Al-Si-5 vol. % WC and Al-Si-5 vol. % $Zro_{2,}$ respectively. The disc material was SAE 1045 steel with hardness HRC 60. The surface roughness (*Ra*) of the wear test specimens and steel disk before the test was measured mechanically using Hommel Tester T_2 (stylus method) was found to be 0.4 and 0.3μm, respectively. The track radius was kept constant at 15mm and the disc speed was maintained at 600 RPM, resulting in a constant sliding velocity of 0.94 m/s. The loads that have been applied in the test were varied between 18 and 180 N corresponding to nominal stress levels of 0.64 and 6.37 MPa, respectively. The sliding wear tests were carried out without interruption for 1 h. The relative humidity was 30% and the initial temperature was (22ºC) for all the tests. Within few minutes into the test, it was observed that the track was smeared with dark debris. The temperature at 2mm below the surface of the pin (using a chromel-alumel thermocouple) was recorded. Prior to testing, samples were cleaned in acetone in an ultrasonic cleaner, dried and weighted using an electronic balance having a resolution of 0.01 mg. After the test, the pins were removed, cleaned in acetone, dried and weighted again to estimate the cumulative weight loss. Calculation of the weight loss was performed by measuring the difference in weight of specimen before and after the test. The density that was measured of the investigated materials were 2.67, 3.27 and 2.8, g/cm^3 for the Al-Si, Al-Si +5 vol.% WC and Al-Si +5 vol.% Zro_2. The wear rate [W (mm^3/m)] was calculated by using the formula, $[W = \Delta W / \rho \times D]$. where: ($\Delta W$) is the weight loss (g), (ρ) is the density (g/cm^3) and (D) is the sliding

distance (m). The worn surfaces of the pins were examined after the wear tests using scanning electron microscopy (SEM). The microstructure of the Al-Si alloy reinforced with either 5 vol. % WC or ZrO_2 is presented in Figure 2.6 (b, c). It can be seen that the WC or ZrO_2 particles in both composites present irregular shapes with sharp corners. The composites show no sign of porosity and exhibit random distribution of particles throughout the matrix. The silicon phase in the matrix of the composites is finer than that of the unreinforced alloy Figure 2.6. (a). It is also observed that the particles are located in the inter dendrite regions and associated with silicon phase Figure 2.6.(d).

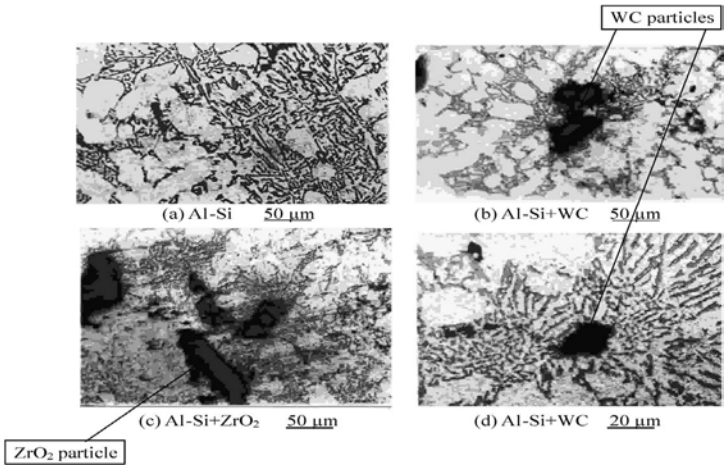

Fig 2.6: Microstructures of the Al-Si matrix alloy and composites. (Daoud et al.2004).

Figure 2.7 shows the relationship between contact surface temperatures at load of (90 N) versus sliding distance for matrix alloy and composites. Both the unreinforced alloy and composites show a continuous increase in temperature with the sliding distance, the rate of increase in temperature being higher for the unreinforced alloy than for the composites. In Table 2.2 the contact temperature reached after a sliding distance of 1800 m, are presented against the applied load.

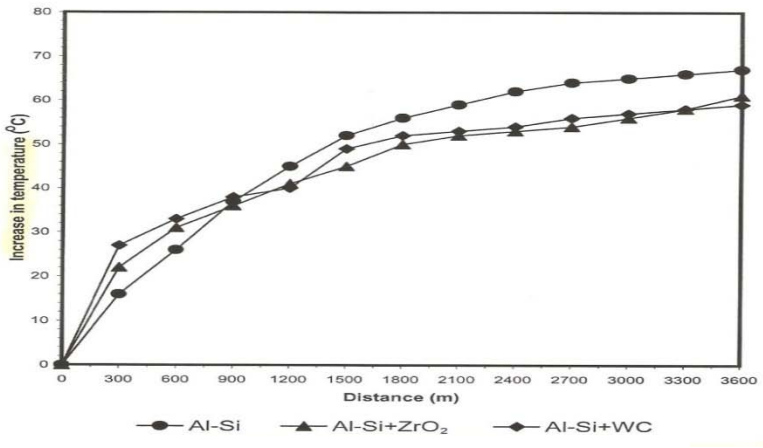

Fig. 2.7: Variation of pin surface temperature with sliding distance for matrix alloy and composites (test load: 90 N). (Daoud et al.2004).

Table 2.2: Variations of temperature and coefficient of friction at different loads of the unreinforced alloy and composites after sliding distance of 1800 m (0.5h). (Daoud et al.2004).

Alloy	Increase in temperature (°C)						Coefficient of friction (f)					
	Load (N)											
	18	36	90	120	150	180	18	36	90	120	150	180
Al–Si	21	21	56	62	74	136	0.3	0.32	0.3	0.37	0.4	0.47
Al–Si+5 vol.%ZrO2	11	24	50	61	71	120	0.37	0.29	0.25	0.39	0.42	0.48
Al–Si+5 vol.%WC	11	21	52	59	69	100	0.27	0.25	0.22	0.38	0.43	0.5

It can be seen in Figure 2.8 and Table.2.2 that the coefficient of friction for all the tested materials decreased with increasing applied load at the load of 18-90N. However, at load above 90N, the coefficient of friction increased as the load increased Daoud et al. (2004).

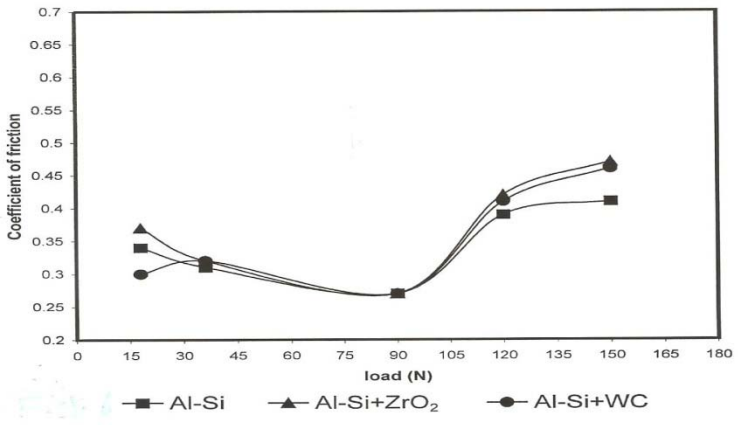

Fig.2.8: Relationship between coefficient of friction and load.(Daoud et al. 2004).

A commercial grade Al-Si eutectic alloy (JIS-AC8A) was used in this study. The elemental composition of JIS-AC8A is given as follows: 12% Si, 0.8% Fe, 1.1% Cu, 1.0%Mg, 1.2% Ni and the balance is aluminum. The Al-Si alloy-graphite composite sample contained 55 vol% graphite. Wear experiments were performed with a three-pin-on-disk apparatus. The three pins were mounted onto a circular holder such that they were equidistant from the center with an angular spacing of 120º. The counter face was machined from a cast iron (JIS-FC250). The total apparent contact area between the three pins and the counter face was 75mm^2. Sand paper size 1500 grade was used to polish the pins and the counter face after that they were cleaned and greased with acetone before each test. The entire test apparatus was placed inside a 275 l environmental chamber. The magnitude of moisture inside the chamber could be varied from 1-100% RH by flowing a mixture of dry air (100 ppm moisture content) and saturated air at 21ºC. Experiments were conducted at 1%, 30%, 50%,70%, and 95% RH. A load range of 25-95 N was used in this study. The relative speed between the pins and counter face was maintained constant at 5 cm/s. A sliding distance of 1 km was used for

each set of experimental parameters. The coefficient of friction was calculated from the averaged friction force and the total wear of the three pins was determined from weight loss measurements. By using Hitachi S4100 scanning electron microscope, worn surfaces and debris were examined and any existence of oxide particles could be detected readily. Many researchers have been reported the formation of a dark layer with a thickness of 1- 10 μm on the rubbing surface of Al-Si alloys. The energy-dispersive X-ray micro-analysis was done at 20 *kv* to give an effective analytical depth of 1-3μm. In addition to the elemental analysis by EDXS, by XRD (Cu *kα* radiation), the composition of the wear debris was analyzed. Figure 2.9 shows the variation of wear rate and friction coefficient with load. The coefficient of friction remains relatively constant while the wear rate increases linearly with load. In 50% RH air and the load range of 25-95 N, the wear loss of the alloy increases linearly with sliding distance and load, which is consistent with the adhesive wear law for metals proposed by many researchers. No load induced wear transition has been observed in the load range examined. In Figure 2.9, the results from Bai(11) and Biswas (11) are also shown for comparison. Both the wear rate and the coefficient of friction found in this study are comparable to that of Bai and Biswas, whose experiments were conducted with a hardened steel counter face in 40% RH air Yen and Ishihara. (1996).

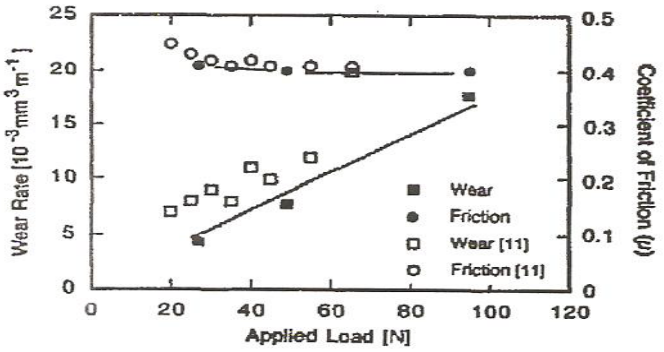

Fig 2.9: variation of friction and wear rate load for Al-Si eutectic alloy in 50% RH air. Results from Bai,Biswas [11] are shown for comparison(Yen and Ishihara 1996).

A pin-on-disc machine was used in dry conditions to conduct these experiments by sliding A 356 Al-30 wt, % SiCp composite with an average particle size of 40 μm as pin material against an EN32 steel disc (the surface roughness was 0.3 μm CLA and hardness of 60 HRC). Load cell and linear variable differential transformer (LVDT) were used to measure the frictional force and wear (displacement) respectively. The coefficient of friction (μ) was calculated by dividing frictional force by normal load, the wear rate by volume loss per sliding distance. The composite had a hardness of 55 HV (at 10 kgf load). All the experiments were conducted using a track diameter of 113mm and they were repeated thrice to check for reproducibility. The magnitude of an applied pressure in all the tests was 2MPa and the speed range of 0.5 to 10.0m/s (0.5, 1, 1.5, 2, 4, 6, 8,10m/s) at ambient conditions of approximately 25 °C and 40-60% relative humidity. At a lower speed (≤2m/s), the frictional force exhibited periodic oscillations with time. The oscillations were characterized by high and low frictional force and were designated as HF and LF respectively. The duration of dwell time at HF position kept on increasing while at LF position it kept on decreasing. Figure 2.10 below shows coefficient of

friction as a function of speed. At speed ≤ 2m/s, coefficient of friction corresponding to HF and LF is superimposed and shown as two separate curves. At 4m/s, oscillations vanish resulting in a constant frictional force with time Ravikiran and Surappa. (1997).

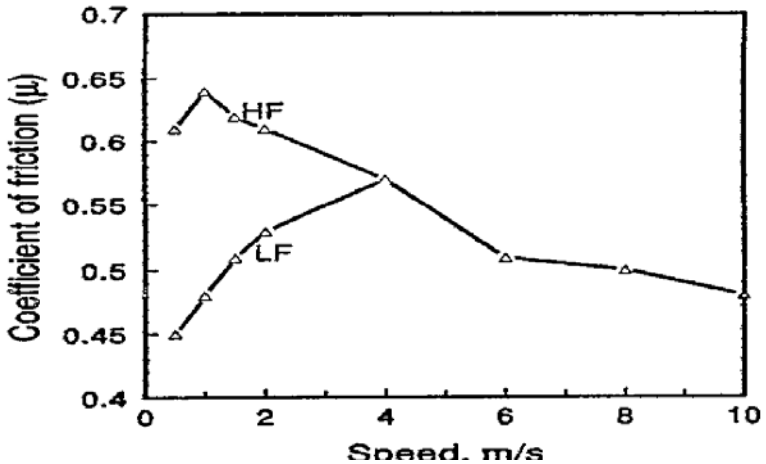

Fig.2.10: Variation in the coefficient of friction with speed.(Ravikiran and Surappa 1997).

Sliding wear behavior of low carbon steel coatings deposited on 319 Al alloy substrates using a plasma transfer wire arc (PTWA) thermal spraying process was studied. Wear tests were performed using a pin-on-disc type wear tester within a load range of 10-75N and a sliding speed range of 0.2-2.5m/s against tool steel pins in a dry air atmosphere (7-10% RH).The frictional forces, and surface temperatures were measured as a function of the applied load and sliding speed . Figure 2.11 below shows the relationship and behavior of the coefficient of friction and temperature with different loads. It is clear that coefficient of friction (COF) was decreased while the load was increased. As shown in Figure 2.11, the surface temperature increased when the load was increased to 340°C at 75 N Edrisy et al. (2001).

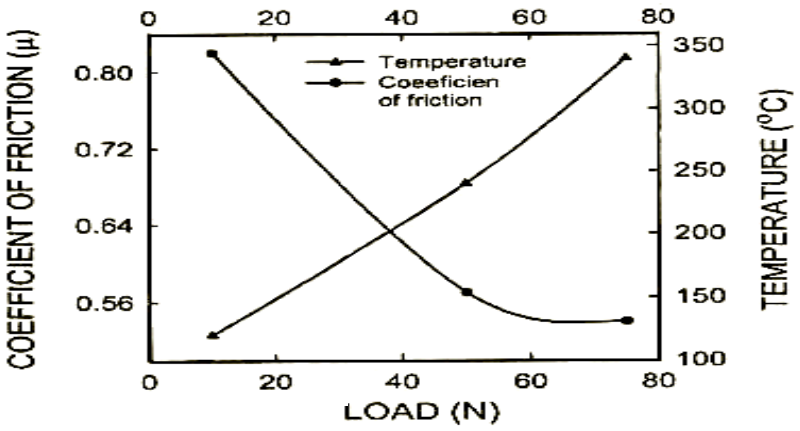

Fig. 2.11: The variation of the friction induced temperature rise of the pin and the coefficient of friction with normal load for samples tested at constant velocity of 2.5m/s. (Edrisy et al.2001).

A pin-on-disk tribometer apparatus was used to investigate the friction and wear properties of Ti (CN)/1045 steel rubbing pairs under dry and lubricated conditions. The range of speed was 0.8 to3.2 m/s and the range of load was 58.8 to 235.2 N. For the lubrication, distilled water and mineral oil (no additives) were used respectively. The tests of wear were conducted on a pin-on-disk tribometer. The pin specimen was fixed and the disk specimen, driven by a motor, could rotate at a different speed. Figure 2.12 shows the schematic diagram of the tester. The initial line contact model was formed between the pin and the disk, which could simulate well the contact form of cutting tool and work-piece in real cutting practice. The angle of inclination of the pin is 80º, so to calculate the wear, an equation was used where: Wear volume = 0.5 L_w $B^2 \times$ $sin\ 10º cos\ 10º$. In this formula, L_w represents the length of ceramic wear scar (5 min this test) and B represent the width of the wear scar (mm). The above formula can be simplified as: $V_w = 0.427\ B^2\ (mm^3)$

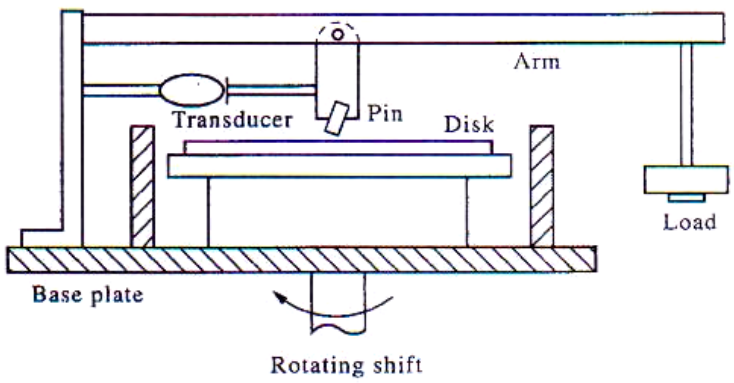

Fig. 2.12: Scheme of contact model of the specimens (Xingzhong et al. 1997).

The pin was made from hot pressed Ti(CN) ceramic, having a size of 5×5×25mm; the disk was machined from 1045 steel (oil quenched, 605 HV in hardness), 50mm in diameter and 6mm in thickness. Surface roughness of the pin and the disk was Ra=0.32 μm and Ra= 0.21 μm, respectively. Table 2.3 below shows some properties of the Ti (CN) ceramic.

Table2.3: Physical and mechanical properties of Ti(N) ceramic.(Xingzhong et al. 1997).

Properties	Unit	Value
Amount	Wt.%	> 80
Grain size	μm	< 1
Density	$g.cm^{-3}$	4.88
Hardness	HV	1540
Bending strength	MPa	750
Fracture toughness	$MPa.m^{½}$	4.7
Impurities		Al_2O_3. ZrO_2

The tests of friction and wear were conducted at room temperature of about 20ºC, under dry and lubricated conditions. For lubrication, distilled water and mineral oil were used. The kinetic viscosity of the pure mineral oil was $30mm^2/s$ at 25ºC. From a reservoir, the

oil and water were fed by natural falling flow during the operating process to the point of contact between the pin and the disk. The average rate of flow was about 0.01 l/min. The range of sliding speed was about 0.8-3.2m/s, and the load about 58.8-235.2N between the rubbing surfaces. The work's time for each pair was 30 min. with the selected speed and load. Every specimen was cleaned ultrasonically in an acetone bath before and after the testing. A transducer was used to transmit the friction force during the test to recorder continuously, from which the friction coefficient could be obtained. The variation of friction coefficient of Ti (CN)/1045 steel pairs with load is shown in Figure 2.13. The sliding speed was 1.6 m/s. It is clear that under dry conditions, (COF) remains constant as a whole when the load is raised. But under lubrication conditions, the coefficient of friction increases gradually and the value of COF is much lower when oil is used as a lubricant.

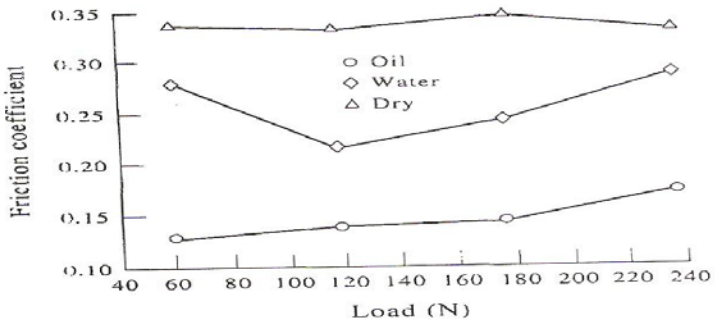

Fig. 2.13: variation of friction coefficient with load. (Xingzhong et al. 1997).

In dry conditions, the most material transfer from steel to ceramic was found, as a result for this statement obtaining rise to the highest friction coefficient of Ti (CN) through the tests. In dry conditions, the friction coefficient is independent of load, which is attributable to the adhesion occurring throughout the whole load range. This result

corresponds well with Amontons First law. Also, the variation of (COF) with different speeds, the load was 117.6N as shown in Figures 2.14. It is clear that the coefficient of friction in dry conditions was higher than the (COF) in the lubricant conditions. And high temperature accelerated the diffusion between the surfaces, and thus brought about very intense adhesion and increased the friction coefficient. Both oil and water improved the friction coefficient in lubricated conditions, especially at high speeds, the oil being more effective. The properties of oil as a cooling, lubrication fluid may have caused the reduction of the friction coefficient Xingzhong et al. (1997).

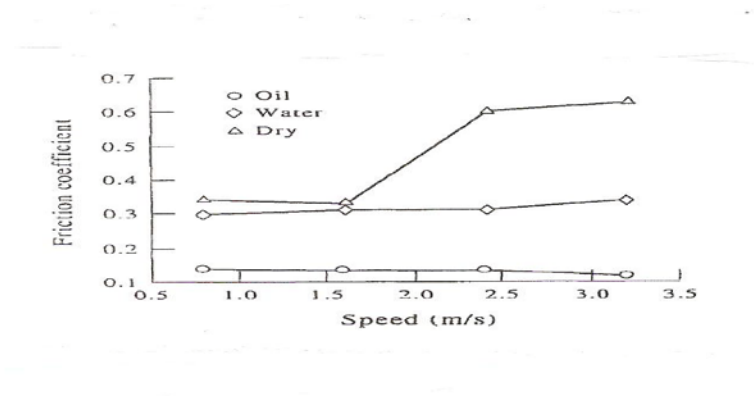

Fig.2.14: variation of friction coefficient with speed. (Xingzhong et al.1997).

To measure friction and wear a universal micro tribometer apparatus was used in this study and it is equipped with a computerized data acquisition system. A crank mechanism formed the essential oscillatory motion. It was designed to be able to change the displacement amplitude. Sinusoidal reciprocating motion was provided by a variable-speed servomotor. Figure 2.15 shows the schematic diagram of the device.

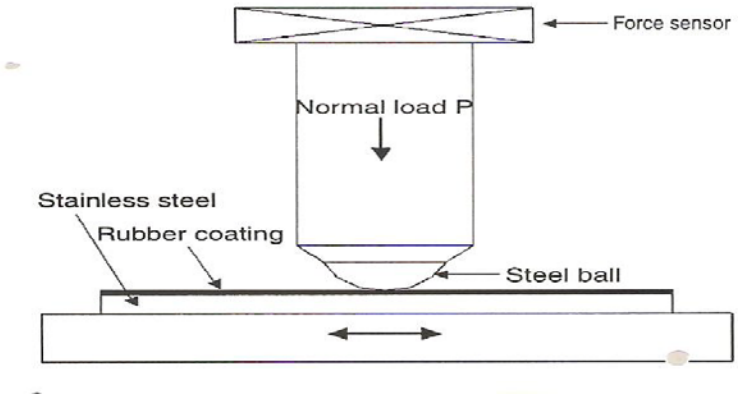

Fig.2.15: Experimental apparatus.(Dae Kyun Baek and Khonsari.2005).

A normal and tangential force were measured by piezo- force sensor. The resolution of the force sensor was 0.01N. The load axis is controlled within 1μm by servomotor. Servomotor controlled the displacement and the rotating revolution per minute within 1μm and 0.02 rpm, respectively. The type of rubber was fluoropolymer. The typical properties of this material based on 1, 90 mm thick slab were: shore hardness (HAS) of 66 MPa and tensile strength of 5.17 MPa. A stainless steel ball used was of the same material as the plates in all the tests. Its diameter and surface roughness (Ra) were 10mm and 0.02μm, respectively. The variation of velocity, normal force and displacement amplitude was recorded in order to investigate the friction and wear of rubber coatings. All the experimental tests were conducted at a constant temperature of 20ºC and RH of 40-50%. Figure 2.16 shows the relationship between the coefficient of friction and the load, these results correspond to the friction at the middle of the stroke. It is clear that coefficient of friction of fresh rubber decreases in a non-linear when the load increases. Dae Kyun Baek and Khonsari.(2005).

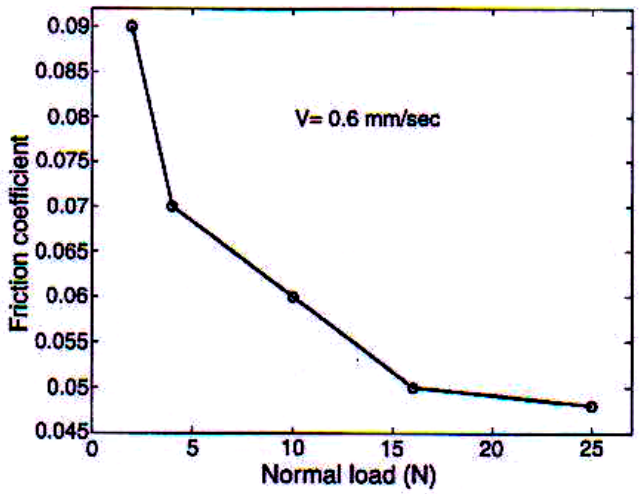

Fig.2.16: Friction coefficient of fresh rubber as a function of load. (Dae Kyun Baek and Khonsari, 2005).

In this study, different types of alloys like Fe_3Si, Fe_3Si alloys containing Cu were fabricated by arc melting, followed by hot-pressing. An investigation on friction and wear behaviors of Fe_3Si based alloys with and without Cu addition against Si_3N_4 ball in water-lubrication was conducted. By arc melting in a water-cooled copper crucible with argon protection Fe_3Si, Fe_3Si-5%Cu and Fe_3Si-10%Cu were fabricated. Each specimen was melted and solidified at least three times to ensure the chemical homogeneity of constituent element is in liquid phase. Electrical discharge method was used to cut the commercial stainless steel AISI 304 into the same size as that of Fe_3Si based alloy. The counterpart was made of Si_3N_4 ceramic ball with a diameter of 9.525mm (available from Shanghai Research Institute of Materials, China). The surface roughness Ra of the Si_3N_4 ball was about 0.02μm. Before each tribological test, the surface of the disks was polished to a surface roughness Ra of about 0.02μm. The Vickers hardness of all the materials used in this investigation was listed in Table 2.4 below.